Proceedings of the 21st ICSMGE, Vienna, Austria, 14 – 19 June 2026. Pistrol, Adam & Schweiger (eds.)
Published by: ÖGG, Austrian Society for Geomechanics, Salzburg, Austria, ISBN 978-3-9503898-4-5
https://doi.org/10.53243/ICSMGE2026-1085

Impact of PSNP Co-injection on Microbially Induced Calcite Precipitation

Yongjoon Choe*, Shaivan H. Shivaprakash, and Susan E. Burns
*School of Civil and Environmental Engineering, Georgia Institute of Technology, Atlanta, GA, *ychoe31@gatech.edu*

ABSTRACT: Micro- and nanosized plastic debris, particularly nanoplastics, have become widespread contaminants in soils, potentially impacting soil improvement and remediation technologies. This study investigated the effects of carboxylated polystyrene nanoplastics (PSNPs) on microbially induced calcite precipitation (MICP), a promising bio-mediated soil stabilization technique. MICP experiments were performed in sand columns with and without the addition of PSNPs. Results indicated that PSNP injection reduced total calcite precipitation by approximately 5.5% and decreased soil stiffness, as indicated by up to an 11% reduction in shear wave velocity. Batch kinetic tests, SEM imaging, and zeta potential analyses suggested that PSNPs preferentially accumulated on sand particle surfaces during the initial stages of biostimulation and cementation. SEM images revealed PSNP particles encapsulated within calcite crystals, indicating incorporation during calcite growth. This research highlights the potential negative impact of nanoplastic contamination on bio-mediated soil stabilization processes, emphasizing the need for further investigation into the mechanisms of interaction between nanoplastics, calcium ions, and biogenic calcite precipitation.

KEYWORDS: Nanoplastics, Microbially Induced Calcite Precipitation, Carboxylated polystyrene.

1 INTRODUCTION

Micro to nanosized plastic debris, originating from the physicochemical degradation of larger plastic waste, have emerged as major pollutants (Sajjad et al. 2022). These particles undergo surface functionalization and fragmentation into nanoscale forms that accumulate in coastal areas (Barnes et al. 2009; Moore et al. 2011; Payel et al. 2025; Sajjad et al. 2022). These nanoplastics interact with various soil constituents, altering the chemical and biological activity in soils (Yu et al. 2021). Consequently, it is essential to consider the presence and impact of nanoplastics on bio-mediated techniques for ground improvement, soil and groundwater remediation. Microbially induced calcite precipitation (MICP) is one such bio-mediated soil stabilization technique which is regarded as a promising method for improving the stiffness of loose sandy soils. In the MICP process, ureolytic bacteria hydrolyze urea to produce ammonia, which increases the pH and triggers calcite precipitation from a dissolved calcium source, thereby binding soil particles together and enhancing its stiffness (Chu et al. 2012, 2014; Dejong et al. 2006; DeJong et al. 2014; Dhami et al. 2013; Lin et al. 2016; El Mountassir et al. 2018; Mujah et al. 2017; Shahin et al. 2020).

Previous studies have reported that heterogeneous particles with negatively charged surfaces can serve as nucleation sites for calcite crystallization (growth). For example, bacteria that provide urease during the MICP process have been shown to possess negatively charged surface due to functional groups, thereby acting as nucleation sites (Fu et al. 2023; Ghosh et al. 2019; Stocks-Fischer et al. 1999). Additionally, micro-sized clay mineral, kaolinite, with negatively charged surfaces have also been reported to act as calcite growth sites, increasing the amount of calcite precipitation (Won et al. 2021). However, it has also been shown that a negatively charged surface alone is not sufficient as a substrate for the growth of calcite precipitation (Zhang et al. 2018). As mentioned earlier, MICP stably precipitates in soils, which typically shows negative surface charge. However, if nanoplastics, which shows negative charge, are not suitable as substrates for calcite growth, the abundant presence of nanoplastics on soil particle surfaces may influence calcite growth.

Therefore, this study aims to evaluate the impact of negatively charged nanoplastics on calcite precipitation, soil stiffness, and microstructure by co-injecting nanosized polystyrene with MICP treatment solutions in sand column experiments. MICP column experiments were conducted with and without nanoplastics, and precipitated calcite profiles, shear wave velocity (V_s), and SEM imaging were used to evaluate the effect of negatively charged nanoplastics on the MICP process. Zeta potential measurement, batch kinetic tests, and DFT-based binding energy calculations were performed to identify the underlying mechanisms of calcite reduction.

2 MATERIALS AND METHODS

2.1 *Materials*

The Ottawa F75 sand was employed as sand column material, which was washed with deionized water and oven-dried at 105 °C. Negatively charged polystyrene microspheres with carboxyl groups (PSNPs) were used as model nanoplastics, having an average diameter of 0.1 µm (range: 0.09–0.15 µm; SD: 0.010 µm; Thermo Fisher Scientific). A stock suspension of PSNPs was diluted to 20 mg/L, simulating a high level of nanoplastic contamination (Choe et al. 2025). Abiotic calcite (>99.95% $CaCO_3$; Thermo Fisher Scientific) was used in the kinetic tests. Material properties are illustrated in Figure 1 and Table 1.

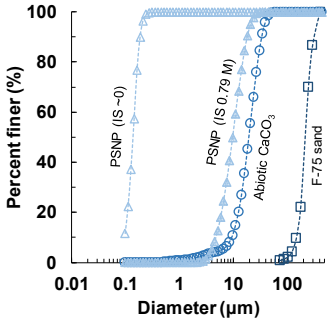

Figure 1. Particle size distribution of tested Ottawa F75 sand specimen for MICP test and abiotic calcite for kinetic batch test.

Table 1. Properties of sand and PSNP used in this study

Material	F75 sand	PSNP
Composition	Quartz (> 99%)	Carboxylated polystyrene
G_s	2.65	0.3
d_{50}	182	0.110 (DI water) 9.90 (IS 0.79 M)
e_{min}, e_{max}	0.49, 0.80	-
Surface density (#/nm^2)	10.6	0.216

Note: G_s (specific gravity) of the sand was determined by gas pycnometer (Ultrapyc 5000), and G_s of the PSNP was referenced from certificate of analysis (Thermo Fisher Scientific); e_{max} (maximum void ratio) and e_{min} (minimum void ratio) of the sand were determined using the funnel-deposition method (ASTM D4254) and the vibrating-table method (ASTM D4253). Surface density for Ottawa F75 sand was estimated based on literature-reported silanol densities on α-quartz surfaces, a crystalline polymorph of SiO_2 (Tang et al. 2015).

2.2 *MICP experiments*

Two sets of MICP sand column (7.62 cm diameter and 15.24 cm height) experiments were run: one with 20 mg/L PSNPs added to each treatment solution, and one without PSNPs as control. The MICP biostimulation was adopted to enhance urea hydrolysis by indigenous ureolytic microbes (DeJong et al. 2022; Gomez et al. 2018, 2019; Graddy et al. 2021), with each cycle employing bottom-up flow (15 mL/min) of 500 mL (~2 pore volumes) of treatment solution (composition in Table 2). After the 1st stimulation treatment, a period of 48 hours at room temperature was allowed for microbial establishment (Gomez et al. 2018; Lee et al. 2019), which was followed by three more stimulation treatments at every 24-hour interval. A flush solution was then injected to minimize abiotic precipitation, and cementation treatments were carried out at 24-hour interval for 10 days.

V_s was measured before the beginning of every cementation treatment and after the final treatment, using three pairs of horizontally oriented bender elements positioned at 2.54 cm (bottom bender element (BE)), mid-height (mid BE), and 3.81 cm (Top BE) from the top, with an additional pair in the top and bottom caps for vertical V_s measurements. After end of cementation treatments, columns were disassembled, and bio-cemented samples were preserved for precipitated calcite measurements and field emission scanning electron microscopy observations (FE-SEM).

Table 2. Properties of sand and PSNP used in this study

Chemical constituent	Treatment		
	Stimulation	Flush	Cementation
Urea (mM)	350	-	250
NH_4Cl (mM)	100	12.5	12.5
Sodium acetate trihydrate	42.5	42.5	42.5
Yeast extract	2.0	2.0	2.00
$CaCl_2$ (mM)	-	-	250
NaOH	Adjust pH to 9	-	-

2.3 *Assessment of PSNP attachment*

Batch kinetic tests were conducted to evaluate the attachment of PSNPs onto sand and calcite surfaces. The IS (0.79 M) and pH (9) of background solution were modified using $CaCl_2$, NaCl, HCl, and NaOH to simulate MICP treatment conditions. PSNPs were added to achieve a concentration of 20 mg/L and dispersed before the test using ultrasonicator. Then, 5 g of each of the substrate material—F75 sand, calcite, and a binary mixture of F75 sand and calcite (75/25 and 95/5)—was combined with 50 mL of the prepared solution in centrifuge tubes and agitated at 20 rpm for predetermined intervals of 5, 10, 20, 30, 60, 120, and 240 minutes. After each interval, the amount of PSNPs attached to the substrate material was calculated by measuring the concentration of PSNPs (C_{PSNP}) in suspension (Figure 2). The observed data for batch kinetic tests were then fitted to pseudo-first-order (PFO) and pseudo-second-order (PSO) kinetic models:

$$ln(q_e - q_t) = ln(q_e) - k_1 t \quad (1)$$

$$\frac{t}{q_t} = \frac{1}{k_2 q_e^2} + \frac{t}{q_e} \quad (2)$$

Here, q_e and q_t denote the attachment capacities at equilibrium and time t, while k_1 (min^{-1}) and k_2 (g mg^{-1} min^{-1}) are the rate constants for the PFO and PSO models, respectively. The R^2 values for q_t were used as a measure of goodness of fit of two parameters for the PFO and PSO models. In addition to kinetic batch test, zeta potential values for precipitated $CaCO_3$, abiotic $CaCO_3$, and PSNP were measured to compare attachment affinity based on electrostatic repulsion. The zeta potential of the precipitated $CaCO_3$ was measured by first immersing a portion of the MICP-treated sand in deionized water, followed by ultrasonic treatment to detach and disperse the $CaCO_3$ adhered to the sand surface. The sand particles were then removed using a sieve, and the resulting suspension was used for the zeta potential measurement.

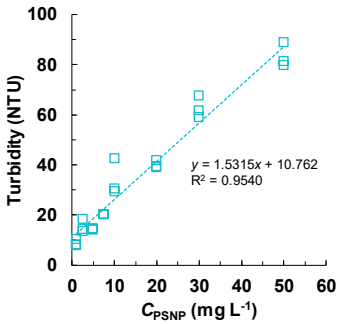

Figure 2. Calibration results for turbidimeter and PSNP concentration.

2.4 *Density functional theory calculations*

Density Functional Theory (DFT) calculations were conducted to quantify and compare the binding affinities of calcite and sand media, representing early-stage interactions during calcite nucleation in MICP systems. Negatively charged silanolate groups (SiO^-) can promote surface-bound nucleation via electrostatic attraction and Ca^{2+} bridging with carbonate (CO_3^{2-}). Accordingly, a simplified model was used in which a single $CaCO_3$ cluster interacts with one deprotonated functional group to approximate local binding affinity at initial nucleation sites. A parallel model for the carboxylate (COO^-) group was built to simulate the interaction between $CaCO_3$ and the surface of PSNPs pre-attached to sand. All computations were performed using the ORCA software package. The hybrid B3LYP functional, combined with the def2-SVP basis set, was employed. Implicit aqueous solvation was considered using the Conductor-like Polarizable Continuum Model (CPCM) to simulate realistic environmental conditions (water, $\varepsilon \approx 78.4$). Geometry optimization and subsequent single-point energy calculations were performed to determine equilibrium structures and final energies. The self-consistent field (SCF) convergence criterion was set to TightSCF (energy change < 1.0×10^{-8} au), and the DFT integration grid was set as ORCA default (defgrid2). For the molecular models, negatively charged functional groups, carboxylate (COO^-) and silanolate ($Si–O^-$), were separately optimized along with a neutral $CaCO_3$ molecular cluster. Binding energies were derived from the difference between the total energies of the complexes (COO^-–$CaCO_3$ and $Si–O^-$–$CaCO_3$) and the sum of the energies of the isolated functional group (COO^- or $Si–O^-$) and $CaCO_3$:

$$\Delta E_{binding} = E_{complex} - (E_{functional\ group} + E_{CaCO_3}) \quad (3)$$

3 EXPERIMENTAL RESULTS

3.1 *Precipitated calcite and Vs profiles*

Figure 3 illustrates the precipitated calcite profiles observed in MICP column experiments. In the column with PSNP injection, the overall calcite content reduced by 5.5% compared to that of the control F75 sand column. Previous MICP studies have reported spatial variability with coefficients of variation ranging from 10-43% within treated columns (Gomez et al. 2019; Shivaprakash et al. 2025). While the observed 5.5% reduction falls within this range of typical experimental variability, the consistency between calcite reduction and V_s reduction (up to 11%) across multiple measurement locations suggests a systematic effect rather than random spatial heterogeneity. Additionally, while the calcite content near the inlet was nearly identical between the two experiments, a slight reduction was observed from mid-height towards the top of the column.

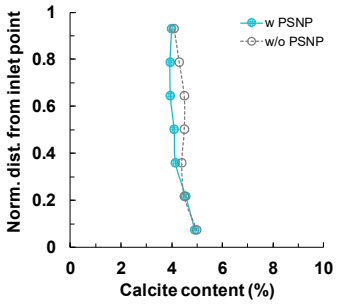

Figure 3. Precipitated calcite profile of tested sand column.

Figure 4 compares the evolution of V_s as a function of cementation treatment in the bio-cemented columns with and without PSNP injection. V_s increased with every cementation cycle, reaching 1069 m/s at the bottom and 861.9 m/s at the top after 10 cycles. The top-bottom BE pair, which reflected the average V_s of the column, showed nearly identical Vs profiles between the columns. PSNP injection reduced V_s by 4.2% with reductions varying by location: 1.6% (top-bottom), 4.7% (bottom), 0.59% (mid), and 11% (top).

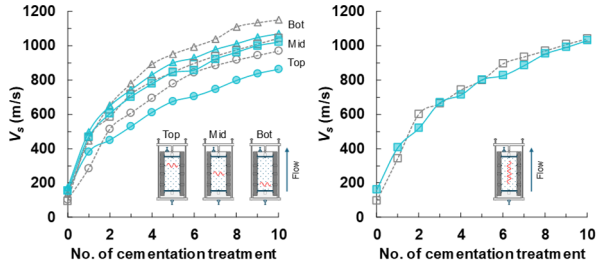

Figure 4. V_s measured from the horizontal BE pairs (left) and the vertical BE pair (right) with respect to cementation cycles. Circle, square, triangle symbols represent the measurements from the top, middle, and bottom BE pairs, respectively. Blue symbols indicate the case where PSNP was co-injected.

3.2 *SEM analysis*

According to SEM observations (Figure 5), a significant amount of PSNP was attached to the sand surfaces in samples collected from the bottom of the column, whereas a smaller amount was observed in samples taken from the top of the column (data not shown here). The attached PSNP was primarily found on the surfaces of sand particles, with minimal presence on bacteria and calcite. Based on representative SEM images, the PSNP attachment per unit surface area of sand was observed to be an average of 0.0091 mg g^{-1} (4.0 particles μm^{-2}) at the lower section and 0.0033 mg g^{-1} (1.4 particles μm^{-2}) at the upper section. Irregular rhombohedrons with trigonal face and pyramidal-like morphologies were observed on the precipitated biotic calcite particles (Figure 5(a-f)), while the abiotic calcite particles in batch kinetic tests were regular rhombohedrons (Figure 5(g and h)), cuboidal or prismatic in shape, as typically observed in literature (Meldrum and Cölfen 2008).

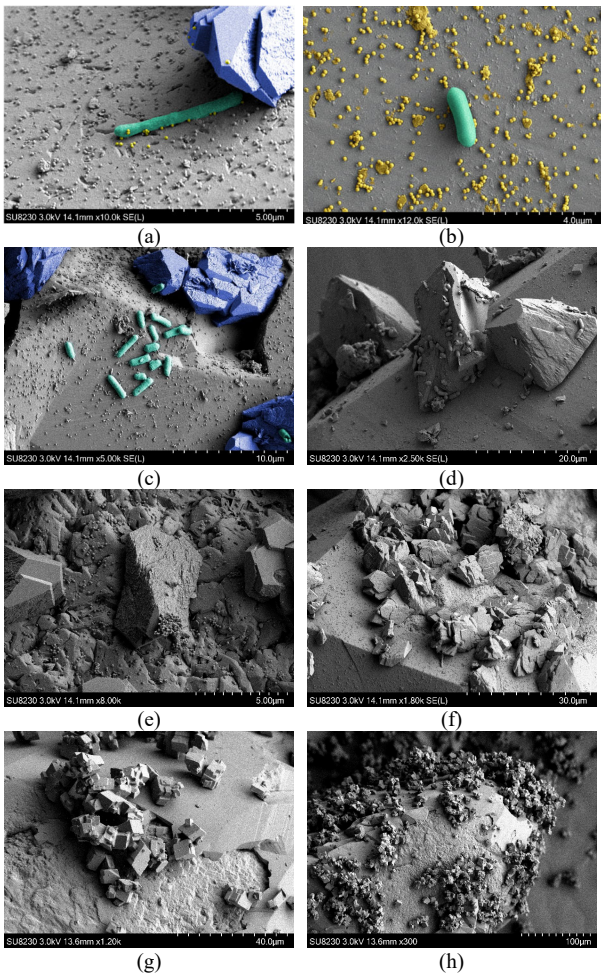

Figure 5. FE-SEM images showing: (a–f) bacterial cells and cell clusters (green), PSNP particles (yellow), and precipitated biotic calcite (blue) on bio-cemented samples obtained from the bottom of the column (a–f). Morphology of abiotic calcite on sand surface samples obtained from batch kinetic tests (g and h).

3.3 *Attachment kinetic of PSNP particles*

Figure 6 presents the results of the batch kinetic test for PSNP. At the concentration of 20 mg/L—used in the MICP experiments—the attachment capacity per time was highest for abiotic calcite and lowest for sand. The equilibrium attachment capacities, q_e, fitted using both PFO and PSO models also showed the highest value for abiotic calcite and the lowest for sand (0.120 mg g^{-1} and 0.215 mg g^{-1} for PFO; 0.129 mg g^{-1} and 0.226 mg g^{-1} for PSO, respectively). In the binary mixture (sand + abiotic calcite), higher attachment capacities were observed when the proportion of calcite was higher and that of sand was lower. The attachment rate for abiotic calcite was either higher than (0.194 vs. 0.129 min^{-1} in PFO) or comparable to that of sand (1.44 in both cases in PSO). Fitted parameters are summarized in Table 3. Figure 7 summarizes the zeta potentials of the materials used in the experiment. The precipitated calcite

and abiotic calcite exhibited relatively similar surface potential values under both deionized water conditions (–23.52 mV and –13.51 mV, respectively) and under IS = 0.79 M conditions (–0.35 mV and –0.96 mV, respectively). The zeta potential of PSNP showed minimal variation with changes in IS.

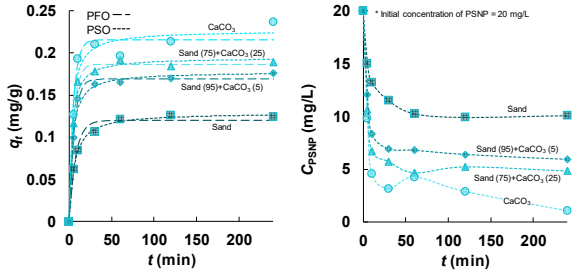

Figure 6. Attachment kinetics of PSNP particles onto sand, abiotic calcite, and binary mixture of sand and abiotic calcite. Attached amount of PSNP at time t (left), and C_{PSNP} over time in supernatant of batch kinetic sample (right).

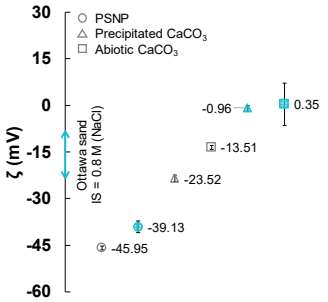

Figure 7. Zeta potentials (ζ) of tested materials. Zeta potential range of Ottawa sand was sourced from Vinogradov et al. (2018). Hollow and blue symbols in (b) indicate measurement under deionized water and 0.79 M, respectively. Error bar indicates standard error of observed values.

Table 3. Fitted results for PSNP kinetic batch test for sand and abiotic calcite.

	PFO			PSO		
	q_e (mg g^{-1})	k_1 (min^{-1})	R^2	q_e (mg g^{-1})	k_2 (g mg^{-1} min^{-1})	R^2
Sand	0.12	0.13	0.98	0.13	1.44	1.00
Sand + calcite 95/5	0.19	0.19	1.00	0.18	1.75	0.99
Sand + calcite 75/25	0.17	0.21	1.00	0.20	1.91	0.99
Calcite	0.22	0.19	0.98	0.23	1.44	0.97

3.4 *Binding energies of single binding sites*

The computed single-site binding energies are summarized in Table 4. Binding energies were calculated as the energy difference between each optimized complex and the sum of its isolated components. The results show slightly stronger binding between COO^- groups and $CaCO_3$ (–49.91 kcal/mol) than between $Si–O^-$ groups and $CaCO_3$ (–44.58 kcal/mol). These values reflect the intrinsic interaction strengths at the molecular scale, independent of functional group density or surface effects.

Table 4. Fitted results for PSNP kinetic batch test for sand and abiotic calcite.

System	Final energy (Hartree)	Binding energy (kcal/mol)
$CaCO_3$	-940.91	-
COO^-	-188.19	-
$Si–O^-$	-364.57	-
COO^-–$CaCO_3$ complex	-1129.1	-49.91
$Si–O^-$–$CaCO_3$ complex	-1305.4	-44.58

4 DISCUSSION

The observed decrease in V_s and the amount of precipitated calcite indicates that the co-injection of PSNPs reduced the overall calcite precipitation. The 5.5% calcite reduction should be interpreted in the context of typical MICP variability. Previous studies have reported spatial coefficients of variation of 10–43% within treated columns (Gomez et al. 2019; Shivaprakash et al. 2025). Although replicate experiments were not performed, the consistency between calcite reduction and Vs reduction (up to 11%) across multiple measurement locations, along with the systematic spatial pattern of reduction toward the column top, suggests a treatment effect rather than random variability.

It is presumed that the PSNPs introduced during co-injection attach to the sand surface, thereby hindering calcite precipitation. Observed PSNP attached to the sand surface (Figure 5(a-f)) suggesting that they continuously accumulated during the stimulation and initial cementation phases. Despite both the sand and PSNPs carrying strong negative charges (Figure 7), the high IS (0.79 M) of the MICP solution appears to have allowed van der Waals attraction to dominate, leading to attachment. If PSNP attachment continued into the later stages of cementation, one would expect some visible attachment of PSNPs on calcite, given the higher attachment rate (k_1 = 0.194 min^{-1}) and attachment capacity (q_e = 0.215 mg g^{-1}) on calcite compared to sand (Table 3). However, SEM images revealed minimal PSNP attachment on calcite surfaces.

As in the case of bacterial cells that become entombed within growing calcite crystals (Figure 5), PSNPs may also have been embedded during cementation, thereby reducing their observable presence on calcite surfaces. Moreover, because urea hydrolysis, nucleation, precipitation, and crystal growth can continue for 4–8 hours after injection of the treatment solution (DeJong et al. 2022), it is plausible that any PSNPs already attached to the sand or existing calcite crystals would be buried during subsequent calcite growth, leaving newly formed crystal surfaces free of PSNPs while allowing further accumulation of PSNPs on the sand.

The effect of PSNPs on bacterial activity was not directly measured. However, bacterial inhibition is unlikely to be the main cause of calcite reduction. Previous studies reported that carboxylated polystyrene nanoplastics were non-toxic to bacteria at concentrations up to 100 mg/L (Heinlaan et al. 2020), and 1 mg/L nanoplastics did not significantly affect bacterial community functions (Zhang et al. 2021). Moreover, if PSNPs inhibited bacterial activity, calcite reduction would be uniform throughout the column, not the gradient pattern observed in Figure 3. Future studies should include direct measurements (e.g., OD600, urease assays) of bacterial activity to confirm this interpretation.

Previous studies (Matijaković Mlinarić et al. 2022; Riddell et al. 2023) have shown that negatively charged surfaces can serve as substrates for heterogeneous nucleation in calcite precipitation. Accordingly, the negatively charged sand surface can induce nucleation through electrostatic attraction with calcium ions. Indeed, biogenically precipitated calcite crystals bound to the sand surface (Figure 5(a-f)) indicate that bacterial cells or the sand surface acted as sites for heterogeneous nucleation. However, following this logic, PSNPs should

enhance calcite precipitation, whereas, as noted above, PSNPs that accumulated on the sand surface during the stimulation phase did not appear to provide a nucleation-friendly environment. This finding contrasts with the assumption that a negatively charged surface of PSNPs would be favorable for calcite nucleation, and is consistent with previous studies showing that neither carboxyl-functionalized PSNPs nor SO_3H-functionalized or unmodified PSNPs facilitated calcite nucleation (Zhang et al. 2018).

The inhibition of calcite precipitation can be attributed to the reduced hydrophilicity of sand particle surfaces. A previous study has demonstrated that media exhibiting neutral or hydrophobic wettability (characterized by high contact angles) significantly reduce calcite precipitation rates compared to hydrophilic media (Tzachristas et al. 2020). In this study, pre-attached PSNP was supposed to reduce the hydrophilicity of certain calcite precipitation sites, thus inhibiting calcite formation. Typically, carboxylated PSNP display high hydrophilicity under pH 3.5–8.5 (Tzachristas et al. 2020). However, under conditions given in MICP, 0.79 M and pH 9, the carboxyl groups (-COOH) undergo deprotonation, transforming into COO–. This alteration results in changes to the surface charge of PSNP and the formation of an unstable hydration layer (Gong et al. 2022). Consequently, the contact angle of PSNP increases, enhancing its hydrophobicity. Note that Ottawa sand generally remains hydrophilic across various IS and pH range (Didier et al. 2015).

In addition, fewer available functional groups on PSNP surface contribute to reducing calcite precipitation sites. Although single molecule binding energy derived from DFT indicated stronger interactions between COO– groups and $CaCO_3$, the functional group density of PSNP used in this experiment was approximately 50 times lower than that of the siloxane groups reported on Ottawa sand (Table 1). Consequently, sand surfaces pre-attached with PSNP exhibited fewer available sites for calcite interaction, and the increased surface roughness due to PSNP attachment further contributed to overall reduced calcite precipitation.

Furthermore, despite biotic and abiotic calcite having nearly identical ζ values under both deionized water and 0.79 M IS conditions, the two types of calcite displayed distinctly different crystal morphologies, highlighting the influence and control of microbial activity on carbonate precipitation. Although abiotic calcite was not precipitated in solution, crystal aggregation and partial attachment of crystals to the sand surface were observed. In contrast, biotically precipitated calcite took the form of individually nucleated crystals that grew to approximately 10–30 μm in size. Most of these biogenic calcite crystals were attached to the sand surface, implying that bacterial cells or the sand itself served as heterogeneous nucleation sites. This contrasts with the kinetic batch experiments, in which no calcite nucleation was observed on the sand surface.

5 CONCLUSION

This study evaluated the effect of carboxylated polystyrene nanoplastics (PSNPs) on microbially induced calcite precipitation (MICP) in sand columns. The addition of 20 mg/L PSNPs during the MICP treatment process led to a 5.5% reduction in overall calcite precipitation and up to an 11% decrease in shear wave velocity. Observed batch kinetic tests and zeta potential measurements implies that PSNPs accumulated on the sand particle surfaces during the initial stimulation and cementation stages. Observed SEM, PSNPs embedded within the calcite crystals, also suggests the possibility that PSNPs adhered to the crystal surface during the calcite growth phase and were subsequently encapsulated by the precipitating calcite. The carboxyl functional groups on the PSNPs covering the sand surface likely interfered with calcite growth, unlike the naturally negatively charged sand particles. Additional studies are required to elucidate the specific interactions between carboxyl groups and calcium ions during calcite formation.

6 REFERENCES

Barnes, D. K. A., F. Galgani, R. C. Thompson, and M. Barlaz. 2009. "Accumulation and fragmentation of plastic debris in global environments." Philosophical Transactions of the Royal Society B: Biological Sciences, 364 (1526): 1985–1998. Royal Society. https://doi.org/10.1098/rstb.2008.0205.

Choe, Y., J. Won, and S. E. Burns. 2025. "Impact of particle size and oxide phase on microplastic transport through iron oxide-coated sand." Water Res, 271. Elsevier Ltd. https://doi.org/10.1016/j.watres.2024.122856.

Chu, J., V. Ivanov, M. Naeimi, V. Stabnikov, and H. L. Liu. 2014. "Optimization of calcium-based bioclogging and biocementation of sand." Acta Geotech, 9 (2): 277–285. https://doi.org/10.1007/s11440-013-0278-8.

Chu, J., V. Stabnikov, and V. Ivanov. 2012. "Microbially Induced Calcium Carbonate Precipitation on Surface or in the Bulk of Soil." Geomicrobiol J, 29 (6): 544–549. https://doi.org/10.1080/01490451.2011.592929.

Dejong, J. T., M. B. Fritzges, and K. Nüsslein. 2006. "Microbially Induced Cementation to Control Sand Response to Undrained Shear." Journal of Geotechnical and Geoenvironmental Engineering, 132 (11): 1381–1392. https://doi.org/10.1061/ASCE1090-02412006132:111381.

DeJong, J. T., M. G. Gomez, A. C. M. S. Pablo, C. M. R. Graddy, D. C. Nelson, M. Lee, K. Ziotopoulou, M. El Kortbawi, B. Montoya, and T.-H. Kwon. 2022. "State of the Art: MICP soil improvement and its application to liquefaction hazard mitigation." Proceedings of the 20th ICSMGE, (1): 405–508.

DeJong, J. T., K. Soga, E. Kavazanjian, S. Burns, L. A. Van Paassen, A. Al Qabany, A. Aydilek, S. S. Bang, M. Burbank, L. F. Caslake, C. Y. Chen, X. Cheng, J. Chu, S. Ciurli, A. Esnault-Filet, S. Fauriel, N. Hamdan, T. Hata, Y. Inagaki, S. Jefferis, M. Kuo, L. Laloui, J. Larrahonda, D. A. C. Manning, B. Martinez, B. M. Montoya, D. C. Nelson, A. Palomino, P. Renforth, J. C. Santamarina, E. A. Seagren, B. Tanyu, M. Tsesarsky, and T. Weaver. 2014. "Biogeochemical processes and geotechnical applications: progress, opportunities and challenges." Bio- and Chemo-Mechanical Processes in Geotechnical Engineering, 143–157. ICE Publishing.

de Souza Machado, A. A., Kloas, W., Zarfl, C., Hempel, S., & Rillig, M. C. (2018). Microplastics as an emerging threat to terrestrial ecosystems. Global change biology, 24(4), 1405-1416.

Dhami, N. K., M. S. Reddy, and A. Mukherjee. 2013. "Biomineralization of calcium carbonates and their engineered applications: a review." Front Microbiol, 4. https://doi.org/10.3389/fmicb.2013.00314.

Didier, M., A. Chaumont, T. Joubert, I. Bondino, and G. Hamon. 2015. "Contradictory trends for smart wate r injection method: role of pH and salinity from sand/oil/brine adhesion maps." Proceedings of the International Symposium of the Society of Core Analysts.

Fu, T., A. C. Saracho, and S. K. Haigh. 2023. "Microbially induced carbonate precipitation (MICP) for soil strengthening: A comprehensive review." Biogeotechnics, 1 (1). KeAi Communications Co. https://doi.org/10.1016/j.bgtech.2023.100002.

Ghosh, T., S. Bhaduri, C. Montemagno, and A. Kumar. 2019. "Sporosarcina pasteurii can form nanoscale calcium carbonate crystals on cell surface." PLoS One, 14 (1). Public Library of Science. https://doi.org/10.1371/journal.pone.0210339.

Gomez, M. G., C. M. R. Graddy, J. T. DeJong, and D. C. Nelson. 2019. "Biogeochemical Changes During Bio-cementation Mediated by Stimulated and Augmented Ureolytic Microorganisms." Sci Rep, 9 (1): 11517. https://doi.org/10.1038/s41598-019-47973-0.

Gomez, M. G., C. M. R. Graddy, J. T. DeJong, D. C. Nelson, and M. Tsesarsky. 2018. "Stimulation of Native Microorganisms for Biocementation in Samples Recovered from Field-Scale

Treatment Depths." Journal of Geotechnical and Geoenvironmental Engineering, 144 (1): 1–13. https://doi.org/10.1061/(ASCE)GT.1943-5606.0001804.

Gong, Y., Y. Bai, D. Zhao, and Q. Wang. 2022. "Aggregation of carboxyl-modified polystyrene nanoplastics in water with aluminum chloride: Structural characterization and theoretical calculation." Water Res, 208. Elsevier Ltd. https://doi.org/10.1016/j.watres.2021.117884.

Graddy, C. M. R., M. G. Gomez, J. T. DeJong, and D. C. Nelson. 2021. "Native Bacterial Community Convergence in Augmented and Stimulated Ureolytic MICP Biocementation." Environ Sci Technol, 55 (15): 10784–10793. https://doi.org/10.1021/acs.est.1c01520.

Heinlaan, M., Kasemets, K., Aruoja, V., Blinova, I., Bondarenko, O., Lukjanova, A., ... & Kahru, A. (2020). Hazard evaluation of polystyrene nanoplastic with nine bioassays did not show particle-specific acute toxicity. Science of the total environment, 707, 136073.

Lee, M., M. G. Gomez, A. C. M. San Pablo, C. M. Kolbus, C. M. R. Graddy, J. T. DeJong, and D. C. Nelson. 2019. "Investigating Ammonium By-product Removal for Ureolytic Bio-cementation Using Meter-scale Experiments." Sci Rep, 9 (1). Nature Research. https://doi.org/10.1038/s41598-019-54666-1.

Lin, H., M. T. Suleiman, D. G. Brown, and E. Kavazanjian. 2016. "Mechanical Behavior of Sands Treated by Microbially Induced Carbonate Precipitation." Journal of Geotechnical and Geoenvironmental Engineering, 142 (2): 1–13. https://doi.org/10.1061/(asce)gt.1943-5606.0001383.

Matijaković Mlinarić, N., A. Selmani, A. L. Brkić, B. Njegić Džakula, D. Kralj, and J. Kontrec. 2022. "Exposure of microplastics to organic matter in waters enhances microplastic encapsulation into calcium carbonate." Environ Chem Lett, 20 (4): 2235−2242. Springer Science and Business Media Deutschland GmbH. https://doi.org/10.1007/s10311-022-01433-w.

Meldrum, F. C., and H. Cölfen. 2008. "Controlling Mineral Morphologies and Structures in Biological and Synthetic Systems." Chem Rev, 108 (11): 4332–4432. https://doi.org/10.1021/cr8002856.

Moore, C. J., G. L. Lattin, and A. F. Zellers. 2011. "Quantity and type of plastic debris flowing from two urban rivers to coastal waters and beaches of Southern California." Journal of Integrated Coastal Zone Management, 11 (1): 65–73.

El Mountassir, G., J. M. Minto, L. A. van Paassen, E. Salifu, and R. J. Lunn. 2018. "Chapter Two - Applications of Microbial Processes in Geotechnical Engineering." Adv Appl Microbiol, G. M. Gadd and S. Sariaslani, eds., 39–91. Academic Press.

Mujah, D., M. A. Shahin, and L. Cheng. 2017. "State-of-the-Art Review of Biocementation by Microbially Induced Calcite Precipitation (MICP) for Soil Stabilization." Geomicrobiol J, 34 (6): 524–537. https://doi.org/10.1080/01490451.2016.1225866.

Payel, S., F. Pahlevani, A. Ghose, and V. Sahajwalla. 2025. "From bulk to bits: understanding the degradation dynamics from plastics to microplastics, geographical influences and analytical approaches." Environ Toxicol Chem. https://doi.org/10.1093/etojnl/vgaf037.

Riddell, J. L., D. J. Vesper, and L. M. Mcdonald. 2023. "Adherence of Polystyrene Microspheres on Cave Sediment: Implications for Organic Contaminants and Microplastics in Karst Systems." Environmental & Engineering Geoscience. https://doi.org/10.1111/EEG-D-22-00090/5900383/10.1111_eeg-d-22-00090.pdf.

Sajjad, M., Q. Huang, S. Khan, M. A. Khan, Y. Liu, J. Wang, F. Lian, Q. Wang, and G. Guo. 2022. "Microplastics in the soil environment: A critical review." Environ Technol Innov. Elsevier B.V.

Shahin, M. A., K. Jamieson, and L. Cheng. 2020. "Microbial-induced carbonate precipitation for coastal erosion mitigation of sandy slopes." Geotechnique Letters, 10 (2): 211–215. ICE Publishing. https://doi.org/10.1680/jgele.19.00093.

Shivaprakash, S. H., Yanez, V. R., Graddy, C. M., Gomez, M. G., DeJong, J. T., & Burns, S. E. (2025). Effect of natural carbonates on microbially induced calcite precipitation process. Scientific Reports, 15(1), 13290.

Stocks-Fischer, S., J. K. Galinat, and S. S. Bang. 1999. "Microbiological precipitation of CaCO 3." Soil Biol Biochem, 31 (11): 1563–1571.

Tang, C., J. Zhu, Z. Li, R. Zhu, Q. Zhou, J. Wei, H. He, and Q. Tao. 2015. "Surface chemistry and reactivity of SiO 2 polymorphs: A comparative study on α-quartz and α-cristobalite." Appl Surf Sci, 355: 1161–1167. Elsevier B.V. https://doi.org/10.1016/j.apsusc.2015.07.214.

Tzachristas, A., R. I. Malamoudis, D. G. Kanellopoulou, E. Skouras, J. Parthenios, P. G. Koutsoukos, C. A. Paraskeva, and V. Sygouni. 2020. "Mineral Scaling in Microchips: Effect of Substrate Wettability on CaCO3Precipitation." Ind Eng Chem Res, 59 (45): 20201–20210. American Chemical Society. https://doi.org/10.1021/acs.iecr.0c03936.

Vinogradov, J., M. D. Jackson, and M. Chamerois. 2018. "Zeta potential in sandpacks: Effect of temperature, electrolyte pH, ionic strength and divalent cations." Colloids Surf A Physicochem Eng Asp, 553: 259–271. Elsevier B.V. https://doi.org/10.1016/j.colsurfa.2018.05.048.

Won, J., B. Jeong, J. Lee, S. Dai, and S. E. Burns. 2021. "Facilitation of microbially induced calcite precipitation with kaolinite nucleation." Geotechnique, 71 (8): 728–734. ICE Publishing. https://doi.org/10.1680/jgeot.19.P.324.

Yu, H., W. Qi, X. Cao, J. Hu, Y. Li, J. Peng, C. Hu, and J. Qu. 2021. "Microplastic residues in wetland ecosystems: Do they truly threaten the plant-microbe-soil system?" Environ Int, 156. Elsevier Ltd. https://doi.org/10.1016/j.envint.2021.106708.

Zhang, W., Y. Ju, Y. Zong, H. Qi, and K. Zhao. 2018. "In Situ Real-Time Study on Dynamics of Microbially Induced Calcium Carbonate Precipitation at a Single-Cell Level." Environ Sci Technol, 52 (16): 9266–9276. American Chemical Society. https://doi.org/10.1021/acs.est.8b02660.

Zhang, Z., Zheng, M., Chen, B., Pan, Y., Yang, Z., & Qian, H. (2021). Nano-sized polystyrene at 1 mg/L concentrations does not show strong disturbance on the freshwater microbial community. Bulletin of Environmental Contamination and Toxicology, 107(4), 610-615.